Hindawi
Advances in Mathematical Physics
Volume 2023, Article ID 9996048, 18 pages
https://doi.org/10.1155/2023/9996048

Research Article

Flow Dynamics of Eyring–Powell Nanofluid on Porous Stretching Cylinder under Magnetic Field and Viscous Dissipation Effects

Ebba Hindebu Rikitu

Department of Applied Mathematics, Adama Science and Technology University, Adama, Ethiopia

Correspondence should be addressed to Ebba Hindebu Rikitu; ebba.hindebu@astu.edu.et

Received 30 May 2023; Revised 11 October 2023; Accepted 3 November 2023; Published 22 November 2023

Academic Editor: Ghulam Rasool

The current paper scrutinized the flow dynamics of Eyring–Powell nanofluid on porous stretching cylinder under the effects of magnetic field and viscous dissipation by employing Cattaneo–Christov theory. In order to study impacts of thermophoretic force and Brownian motion, the two-phase (Buongiorno) model is considered. As a consequence, very nonlinear PDEs that govern flow problem were formulated, transformed into ODEs via relevant similarity variables, as well as tackled by utilizing R-K-45 integration scheme along with the shooting technique in the MATLAB R2018a software. Consequently, the numerical simulations reveal that Eyring–Powell fluid, curvature, velocity ratio parameters have the propensity to raise nanofluid velocity. Nanofluid temperature shows an increasing pattern with magnetic, curvature, dissipative heating, and thermophoresis parameters. Besides, Prandtl number, Eyring–Powell fluid, velocity ratio, thermal relaxation time, and porous parameters indicate the declining impact against the nanofluid temperature. Hence, the porous medium reasonably and successfully managed nanofluid temperature as well as the overall thermal system in terms of system cooling. The concentration profile gets fall down with escalating values of Schmidt number, magnetic, curvature, dissipative heating, thermophoresis, Brownian motion, and solutal relaxation time parameters. Moreover, coefficient of the skin friction gets rise for larger values of Eyring–Powell fluid, magnetic and curvature parameters however porous medium and velocity ratio parameters reveal the opposite trends on it. The magnetic, curvature, Eyring–Powell fluid, velocity ratio, and dissipative heating parameters indicate increasing impacts on both Nusselt *Nu* and Sherwood *Sh* numbers even though both *Nu* and *Sh* get cut down with the porous medium parameter. Moreover, an excellent and sound agreement was attained up on comparing coefficients of the skin friction for the current result against that of previously published literatures under some limiting cases.

1. Introduction

The great scientific breakthrough in fluid mechanics have made non-Newtonian fluids to be very important fluids as a result of their immense applications in biomedical, chemical engineering, and manufacturing industries including food processing, power engineering, petroleum production, paper manufacturing, glass sheet blowing, polymer solutions, and biological gels, etc. [1, 2]. From our real-life encounters, materials like blood, starch suspension, pharmaceuticals, toothpastes, shampoos, paints, cosmetics, butter, honey, etc. are excellent examples of non-Newtonian fluids. Such types of fluids exhibit a property that the shearing stresses are nonlinearly related with the rates of strain. To put it in another way, non-Newtonian fluids possess shear thinning/thickening behaviors and frequently show the yielding stresses by which the shearing stresses are nonlinearly proportional to the deformation rates of strain resulting in so much complicated and complex mathematical analysis [3]. In this perspective, the well-known Navier–Stoke's equations failed to express adequately the prominent characteristics of such fluids. Nowadays, hence, various flow models for the non-Newtonian fluids namely Carreau, Williamson, Maxwell, Micropolar, Casson, Jeffery, Eyring–Powell, etc. have been formulated. Among these fluids, Eyring–Powell [4] fluid model being formulated in 1994 through Eyring and Powell has obtained astonishing considerations because of the facts indicated as follows: first, the model was obtained through liquids kinetic theories rather than the experiential study; second, in the case of higher and lower rates of shearing the model performs as that of the Newtonian fluids but as that of the non-Newtonian fluids in the case of modest rates of shearing.

Now a day, a number of research reports on Eyring–Powell fluid have been communicated. For instance, Ibrahim and Hindebu [5] analyzed MHD boundary layer flow of Eyring–Powell nanofluids using the Cattaneo–Christov heat-mass fluxes theories. The stretching cylinder prompted flow model equations were solved numerically via the Keller-Box technique and they announced that the Nusselt number was augmented with the Prandtl number, curvature parameter, thermal relaxation time, and Eyring–Powell fluid parameter. Meanwhile, Layek et al. [6] investigated the combined transport of heat and mass for unsteady, incompressible, viscous Eyring–Powell fluid along expanding/shrinking sheet with suction/injection, Dufour and Soret effects. According to their results, the fluid velocity is high for the Eyring–Powell fluid but Prandtl number and thermal radiation lessen the fluid temperature. Moreover, analysis of nonlinear stratified convection of Eyring–Powell fluid past a sheet, which is inclined and stretching with Cattaneo–Christov heat-mass flux model is presented by Jabeen et al. [7]. Their analysis revealed that the thermal stratification parameter and Cattaneo–Chiristov time relaxation dampen the distribution of fluid temperature. Salah [8] examined the flow and heat transfer of dissipative and chemically reacting MHD Eyring–Powell fluid past a sheet that stretches in an exponential manner under non-Fourier's model. This examination revealed that the thermal relaxation time and the Eyring–Powell fluid parameter are inversely related to the temperature profile while the Eckert number indicates an increasing effect on the temperature profile. Later on, Akram et al. [9] presented the investigation of double diffusion effect on the flow of MHD Eyring–Powell nanofluid over the channel with not uniform property. Very recently, the analysis of MHD Eyring–Powell fluid convection through a sheet, which stretches in an exponential way was given by Naseem et al. [10]. Their analysis considered the Cattaneo–Christov model and hence, they concluded that both temperature field and thermal boundary layer thickness decline with the time relaxation parameter but both escalate with the Eckert number. It is also noticed that, fluid velocity for the Eyring–Powell is larger than that of the viscous fluid but this is the contrary scenario in the case of the fluid temperature, moreover, the magnetic field revealed the retarding effect on the velocity field but the enhancing effect on the temperature distribution.

Nanofluids are new class of liquids that are engineered via homogeneous mixing of nanometer size (1 nm – 100 nm) solid particles and conventional base liquids namely oils, water, and ethyleneglycol. As far as the solid nanoparticles are concerned, metals, metallic-oxides, and carbides are often used to prepare nanofluids since they possess thermal conductivity larger than that of the common base fluids. Therefore, nanofluids own improved physico-thermal characteristics namely dynamic viscosity, transfer rate of heat, thermal conductivity, and hence they have huge applications in biomedicine like cancer therapy and nanodrug delivery as well as cooling process in the industries namely microelectronics cooling, cooling of microchips in computers, air-craft, vehicle cooling, nuclear reactors cooling, chillers, refrigerators, food processing, paper production, and many others [11]. Nanofluids were introduced and intensively studied by Choi [12] for the first time in 1995. After the pioneering work of Choi, a great deal of research has been explored for the convection of nanofluids over diverse geometries and various aspects in [13–21].

The porous media amalgamation with the nanofluids can further escalates the rates of heat energy transfers for many thermal system managements. Indeed, solid matrixes possessing the interconnected and networked pores/voided spaces through which fluids can flow are referred to as porous media [22]. Peculiar examples of natural porous media include rocks, sands, soils, biological tissues like bones, lungs, and kidneys whereas materials such as bread, sponges, cements, rubber, foams, and ceramics can be considered as man-made porous media. The enhanced thermo-physical properties of nanofluids may further improve because porous medium increases areas of the contacting surfaces among solids and fluid particles so that flow interruptions are increasing. Porous medium flow has many areas of applications including petroleum product filtration, underground water movement, geothermal extraction, crude oil extraction, storage of radioactive nuclear waste, heating and cooling in buildings, solar power collectors, biomedical sciences, and so on [23, 24]. The first description of transport phenomena via porous media was proposed in 1956 through Darcy Henry [25]. At the present time, following Darcy's effortless work, fluid flows over a porous medium are attracting the attention of a prodigious scientific community including [26–32].

Magneto-hydro-dynamics (MHD) is the subject that focuses on the analysis of communal interactions among the imposed magnetic field and the fluid particles that also conduct electrically while in the state of motion such as electrolytes, metal fluids, plasma, and salt water. The phenomenon of MHD plays an outstanding role in medicine, technology, and engineering fields, like in metallurgy, treating of cancer tumors, reactors cooling, welding of plasmas, magnetic cells separation, solidification of magmas, gratings of optical, magnetic drug targeting, devices of astrophysics, measurements of blood flow, and so on [33, 34]. Based on these influencing attributes, currently a great deal of authors from the research and academic world is publishing articles consisting MHD flows under the different scenarios. To mention some, Maxwell nanofluid flow over the vertical sheet that stretches exponentially under second order slip effect, viscous dissipation, radiative heat flux as well as applied Lorentz force was analyzed by Abbas et al. [35] applying Buongiorno's model. The mathematical analysis conducted for Eyring–Powell electrically conducting nanofluid motion created because of wedge surface elongating under the influences of radiative heat, generation of heat, and convectively imposed conditions on the boundaries was done through Raju et al. [36]. Moreover, Arif et al. [37] carried out a numerical study on the investigations of both mass and heat transfers regarding the motion of

Maxwell nanofluid through a heated sheet that also stretches under the impact of applied magnetic field. Similar MHD nanofluids flows are given in the relevant and up-to-date literature [38–46] and the references therein.

Furthermore, the dynamics of mutual influences of Viscous–Joule dissipations have many applications in the thermal transport process of nanofluids over the surfaces with stretching behaviors. The physical interpretation for the viscous-dissipation is that, it is just the rate of energy conversion per unit mass from its kinetic form to that of the thermal one. Concerning this issue, Narender et al. [47] performed a numerical study on heat and mass transport for chemically reacting MHD nanofluid with the influences of viscous-dissipation and radiative heat flux on a stretching sheet. As they declared, both the temperature profile and surface heat transfer rate enhance for flows with higher viscous dissipation. Later on, Abbas and Megahed [48] explored thermal radiation and viscous dissipation effects on the steady flow of Eyring–Powell fluid over a stratified a stretching sheet embedded in a porous medium. The numerical solution was obtained via the Chebyshev spectral method and they pointed out that the temperature profile escalates with the viscous dissipation and porous parameter.

On the other hand, Joule heating (or Ohmic heating) refers to a process of creating excessive heat in nanofluids because of the applied magnetic field. Actually, Joule heating comprises important attributes in the food industry, bulbs, electrolysis, electric fuzes and heaters, conduction of oven, flashlights, etc. In line with this, Olkha and Dadheech [49] scrutinized the impact of Joule heating on the unsteady MHD slip flow of the Eyring–Powell fluid as well as the motile microorganisms across an inclined permeable stretching sheet embedded in porous channel with thermal radiation and thermal sink. Their results revealed that the magnetic and porosity parameters give rise in the thermal heat transfer rate. In addition, the flow and heat transfer characteristics examination of MHD nanofluid using Ag as solid nanoparticles suspended in water with combined dissipation of Viscous–Joule past a cylinder that stretches under the slip conditions at the boundary as well as injection/suction was given by Mishra and Kumar [50]. The numerical solutions were given via R-K-45 along the method of shooting. Thus, the Nusselt number falls down when the magnitudes of viscous dissipation and Joule heating parameters increase. Babu et al. [51] demonstrated the analysis of thermally radiating 2D MHD Eyring–Powell fluid flow over the surface that stretches under a joint impact of Viscous–Joule dissipations. They noticed that enhancing the viscous dissipation as well as the Joule heating parameters enhances the nanofluid temperature distribution. Indeed, a list of up-to-date and relevant references from the literature with regard to the joint influences of Viscous–Joule dissipations is reported by Ramesh et al. [52], Sadighi et al. [53], and Jayanthi and Niranjan [54].

Related literatures abovementioned motivated the current study and therefore, the current study investigates flow as well as mass and heat transport for Eyring–Powell nanofluid on the cylinder that stretches under the applied magnetic field. The survey of related literature established that no such problem has been studied regarding the jointed influences of Viscous–Joule heating caused by dynamic viscosity, applied magnetic field, and porous medium by employing the non-Fourier's heat conduction model which is also known as Cattaneo–Christov heat and mass flux model. Moreover, same boundary conditions were not considered before. The solutions of the current study are given via R-K-45 integration scheme coupled by the method of shooting. As a consequence, parameter-dependent solutions for the velocity profile, temperature profile, concentration profile, wall sear stress, wall heat, and mass transfer rates were investigated as well as displayed through graphs. Moreover, an excellent and sound agreement was attained up on comparing results of the current numerical method coefficient of the skin frictions with the numerical solutions reported by formerly available literatures on behalf of various controlling cases. Therefore, it is a worthwhile attempt and the author believes that the current results are authentic and novel.

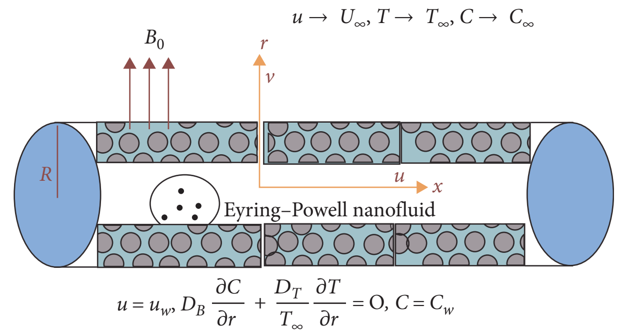

Figure 1: Coordinate system and flow model.

2. Problem Analysis and Mathematical Modeling

Consider a steady, laminar, and viscous two-dimensional MHD Eyring–Powell fluid past a porous cylinder with radius R that stretches in the horizontal direction. Also, consider a polar cylindrical coordinate system (x, r) as exhibited in Figure 1. The flow direction for the Eyring–Powell nanofluid is along x-axis as porous cylinder stretches linearly with the uniform velocity u_w.

Following Powell and Eyring [4], the shear stress for Eyring–Powell model can be written as follows:

$$\tau_{ij} = \mu \frac{\partial u_i}{\partial x_j} + \frac{1}{\beta} \sinh^{-1}\left(\frac{1}{c}\frac{\partial u_i}{\partial x_j}\right) = \mu \frac{\partial u}{\partial r} + \frac{1}{\beta} \sinh^{-1}\left(\frac{1}{c}\frac{\partial u}{\partial r}\right), \tag{1}$$

where τ_{ij} is the Cauchy stress tensor for Eyring–Powell fluid, u is the axial fluid velocity, nd μ is the dynamic viscosity whereas β and c are the rheological Eyring–Powell fluid model parameters. The Taylor's series expansion of $\sinh^{-1}$ approximating to the second-order gives:

$$\sinh^{-1}\left(\frac{1}{c}\frac{\partial u}{\partial r}\right) \approx \frac{1}{c}\frac{\partial u}{\partial r} - \frac{1}{3!}\left(\frac{1}{c}\frac{\partial u}{\partial r}\right)^3, \left|\frac{1}{c}\frac{\partial u}{\partial r}\right| \ll 1. \tag{2}$$

Thus, Equation (1) takes the form as follows:

$$\tau_{ij} = \mu\frac{\partial u}{\partial r} + \frac{1}{\beta c}\frac{\partial u}{\partial r} - \frac{1}{6\beta c^3}\left(\frac{\partial u}{\partial r}\right)^3. \tag{3}$$

Moreover, it is assumed that a uniform magnetic field B_0 is imposed opposite to the flow direction. The uniform surface temperature T_w and surface concentration C_w are considered while T_∞ and C_∞ are temperature and concentration in the free stream, respectively. The induced magnetic field is considered as negligible when compared to the applied magnetic flux because of extremely small magnetic Reynolds number. Besides, consider a homogeneous and isotropic porous and two-phase Buongiorno model for nanofluids is applied in formulating the energy and concentration equations. The zero net surface mass flux of the nanoparticles is considered. More importantly, instead of classical Fourier's and Fick's diffusion models, the frame indifferent Cattaneo–Chiristov diffusion model is considered.

Following the study by Christov [55], the Cattaneo–Christov heat-mass flux model instead of the Fourier's and Fick's models can be written as follows:

$$\lambda_E\left[\frac{\partial q}{\partial t} + U.\nabla q - q.\nabla U + (\nabla.U)q\right] + q = -k\nabla T, \tag{4}$$

$$\lambda_C\left[\frac{\partial J}{\partial t} + U.\nabla J - J.\nabla U + (\nabla.U)J\right] + J = -D_B\nabla C, \tag{5}$$

where $U=(u, v)$ represent the fluid velocity vector, q is heat flux, J is mass flux, λ_E denotes the thermal relaxation time, λ_C denotes the solutal relaxation time, k is fluid thermal conductivity, and D_B stands for molecular mass diffusivity of the species, It is noteworthy that for $\lambda_E=\lambda_C=0$, Equations (4) and (5) are simplified to the classical Fourier's and Fick's laws, respectively.

For steady incompressible fluid flow, Equations (4) and (5) reduce to:

$$\lambda_E[U.\nabla q - q.\nabla U] + q = -k\nabla T, \tag{6}$$

$$\lambda_C[U.\nabla J - J.\nabla U] + J = -D_B\nabla C. \tag{7}$$

Under the aforementioned considerations, the boundary-layer PDEs are formulated and hence written according to the following equations:

$$\frac{\partial(ru)}{\partial x} + \frac{\partial(rv)}{\partial r} = 0, \tag{8}$$

$$\begin{aligned} u\frac{\partial u}{\partial x} + v\frac{\partial u}{\partial r} &= \frac{\mu}{\rho}\left(\frac{\partial^2 u}{\partial r^2} + \frac{1}{r}\frac{\partial u}{\partial r}\right) + \frac{1}{\rho\beta c}\left(\frac{\partial^2 u}{\partial r^2} + \frac{1}{r}\frac{\partial u}{\partial r}\right) \\ &- \frac{1}{6\rho\beta c^3}\left[\frac{1}{r}\left(\frac{\partial u}{\partial r}\right)^3 + 3\left(\frac{\partial u}{\partial r}\right)^2\frac{\partial^2 u}{\partial r^2}\right] - \frac{\sigma}{\rho}{B_0}^2 u - \frac{\mu}{\rho k_0}u, \end{aligned} \tag{9}$$

$$\begin{aligned} u\frac{\partial T}{\partial x} + v\frac{\partial T}{\partial r} &= \alpha_f\left(\frac{\partial^2 T}{\partial r^2} + \frac{1}{r}\frac{\partial T}{\partial r}\right) + Đ^3\left[D_B\frac{\partial C}{\partial y}\frac{\partial T}{\partial y} + \frac{D_T}{T_\infty}\left(\frac{\partial T}{\partial y}\right)^2\right] + \lambda_E\left[u^2\frac{\partial^2 T}{\partial x^2} + v^2\frac{\partial^2 T}{\partial r^2} + 2uv\frac{\partial^2 T}{\partial x\partial r} + u\frac{\partial u}{\partial x}\frac{\partial T}{\partial x} + u\frac{\partial v}{\partial x}\frac{\partial T}{\partial r}\right. \\ &\left.+ v\frac{\partial u}{\partial r}\frac{\partial T}{\partial x} + v\frac{\partial v}{\partial r}\frac{\partial T}{\partial r}\right] + \frac{1}{\rho c_p}\left[\left(\mu + \frac{1}{\beta c}\right)\left(\frac{\partial u}{\partial r}\right)^2 - \frac{1}{6\beta c^3}\left(\frac{\partial u}{\partial r}\right)^4\right] + \frac{\sigma {B_0}^2}{\rho c_p}u^2 + \frac{\mu}{\rho c_p k_0}u^2, \end{aligned} \tag{10}$$

$$\begin{aligned} u\frac{\partial C}{\partial x} + v\frac{\partial C}{\partial r} &= D_B\left(\frac{\partial^2 C}{\partial r^2} + \frac{1}{r}\frac{\partial C}{\partial r}\right) + \frac{D_T}{T_\infty}\left[\frac{\partial^2 T}{\partial r^2} + \frac{1}{r}\frac{\partial T}{\partial r}\right] + +\lambda_C\left[u^2\frac{\partial^2 C}{\partial x^2} + v^2\frac{\partial^2 C}{\partial r^2} + 2uv\frac{\partial^2 C}{\partial x\partial r} + u\frac{\partial u}{\partial x}\frac{\partial C}{\partial x} + u\frac{\partial v}{\partial x}\frac{\partial C}{\partial r}\right. \\ &\left.+ v\frac{\partial u}{\partial r}\frac{\partial C}{\partial x} + v\frac{\partial v}{\partial r}\frac{\partial C}{\partial r}\right], \end{aligned} \tag{11}$$

where c_p designates specific heat capacity, D_T thermophoretic diffusion coefficient, $Đ^3 = \frac{(\rho c_p)_p}{(\rho c_p)_f}$ is heat capacity ratio, $(\rho c_p)_p$ is nanoparticles heat capacity, and $(\rho c_p)_f$ represents base fluid heat capacity.

Imposed boundary conditions are:

$$u = u_w(x) = u_0\left(\frac{x}{l}\right), v = 0, T = T_w(x) = T_\infty + T_0\left(\frac{x}{l}\right), D_B\frac{\partial C}{\partial r} + \frac{D_T}{T_\infty}\frac{\partial T}{\partial r} = 0, \text{for } r = R \text{ and } u = u_\infty, v = 0, C = C_\infty, T = T_\infty \text{ as } r \to \infty. \tag{12}$$

To transform Equations (8)–(12) into ODEs the following dimensionless variables are introduced.

$$\eta = \frac{r^2 - R^2}{2R}\sqrt{\frac{u_0}{\nu l}}, \psi = \sqrt{u_w \nu x} R f(\eta), u = u_w f'(\eta), v = -\frac{R}{r}\sqrt{\frac{\nu u_0}{l}} f(\eta), \theta(\eta) = \frac{T - T_\infty}{T_\mathrm{w} - T_\infty}, \phi(\eta) = \frac{C - C_\infty}{C_\mathrm{w} - C_\infty}. \tag{13}$$

Using Equation (13), Equation (8) is automatically satisfied while Equations (9)–(11) are transformed into the following ODEs:

$$(1+\delta)(1+2\gamma\eta)f''' + ff'' - f'^2 + 2\gamma(1+\delta)f'' - \frac{4}{3}\delta\lambda\gamma(1+2\gamma\eta)f''^3 - \delta\lambda(1+2\gamma\eta)^2 f'''f''^2 - (M+K)f' = 0, \tag{14}$$

$$\frac{(1+2\gamma\eta)}{Pr}\theta'' + \frac{2\gamma}{Pr}\theta' + f\theta' - \alpha t(f^2\theta'' + ff'\theta') + Nb(1+2\gamma\eta)\theta'\phi' + Nt(1+2\gamma\eta)\theta'^2 + Ecf''^2\left((1+\delta)(1+2\gamma\eta) - \frac{1}{3}\delta\lambda f''^2\right) + Ec(M+K)f'^2 = 0, \tag{15}$$

$$(1+2\gamma\eta)\phi'' + 2\gamma\phi' + Scf\phi' - Sc\alpha c(f^2\phi'' + ff'\phi') + \frac{Nt}{Nb}[(1+2\gamma\eta)\theta'' + 2\gamma\theta'] = 0, \tag{16}$$

where $\gamma = 1/R\sqrt{\nu l/u_0}$ is the curvature parameter, $\delta = 1/\mu\beta c$ is the Eyring–Powell fluid parameter, $\lambda = {u_0}^3 x^2/2c^2 l^3 \nu$ is the fluid parameter, $M = \sigma {B_0}^2 l/\rho u_0$ is the magnetic parameter, $Pr = \nu/\alpha_f$ is the Prandtl number, $\alpha t = \lambda_E u_0/l$ is the thermal relaxation time parameter, $Nb = Ð^3 D_B(C_\mathrm{w} - C_\infty)/\nu$ is the Brownian motion parameter, $Nt = Ð^3 D_T(T_\mathrm{w} - T_\infty)/\nu T_\infty$ is the thermophoresis parameter, $Sc = \nu/D_B$ is the Schmidt number, $\alpha c = \lambda_C u_0/l$ is the solutal relaxation time parameter, $K = \mu l/u_0 \rho k_0$ is porous parameter, and $Ec = {u_w}^2/c_p(T_\mathrm{w} - T_\infty)$ is the Eckert number (or viscous dissipation parameter).

The imposed boundary conditions in Equation (12) become:

$$f'(0) = 1, f(0) = 0, \theta(0) = 1, Nt\theta'(0) + Nb\phi'(0) = 0, f'(\infty) = A, f(\infty) = 0, \theta(\infty) = 0, \phi(\infty) = 0, \tag{17}$$

where $A = u_\infty/u_w$ is the velocity ratio.

Engineering and industrial interest quantities are the skin friction coefficient, the Nusselt number and the Sherwood number. The skin friction coefficient C_f can be written as follows:

$$C_f = \frac{2\tau_w}{{u_w}^2}. \tag{18}$$

However, τ_w is the wall shear stress and it can be obtained from the Cauchy stress tensor for the Eyring–Powell fluid as follows:

$$\tau_w = \left[\tau_{ij}\right]_{r=R} = \left[\mu \frac{\partial u}{\partial r} + \frac{1}{\beta c}\frac{\partial u}{\partial r} - \frac{1}{6\beta c^3}\left(\frac{\partial u}{\partial r}\right)^3\right]_{r=R}. \tag{19}$$

The nondimensional coefficient of skin friction C_f in Equation (18) takes the form:

$$\frac{1}{2} C_f \sqrt{Re_x} = (1+\delta) f''(0) - \frac{1}{3}\delta\lambda f''^3(0). \tag{20}$$

The wall heat transfer rate or local Nusselt number Nu is defined as follows:

$$Nu = \frac{x q_w}{k(T_w - T_\infty)}, \tag{21}$$

where $q_w = -k(\frac{\partial T}{\partial r})_{r=R}$ represents wall heat–flux. Thus, the nondimensional Nu takes the following form:

$$\frac{Nu_x}{\sqrt{Re_x}} = -\theta'(0). \tag{22}$$

Similarly, the wall mass transfer rate or local Sherwood number Sh is defined as follows:

$$Sh = \frac{x J_w}{D_B(C_w - C_\infty)}, \tag{23}$$

where $J_w = -D_B(\frac{\partial C}{\partial r})_{r=R}$ designates wall mass-flux and thus, the nondimensional form of Sh takes the following form:

$$\frac{Sh_x}{\sqrt{Re_x}} = = -\phi'(0). \tag{24}$$

3. Method of Numerical Solutions

The closed form solutions for the highly nonlinear governing Equations (14)–(16) with boundary conditions Equation (17) are not possible. Hence, this highly nonlinear governing Equations (14)–(17) are numerically solved by using the fourth–fifth order Runge–Kutta–Fehlberg integration scheme in the MATLAB R2018a software. The initial conditions were guessed by utilizing the shooting technique until the boundary conditions were satisfied. Also, in the numerical calculations the maximum step size $\Delta\eta = 0.01$. The criteria used for convergence is the variation in the dimensionless velocity, temperature, and concentration should be less than 10^{-7} between any two consecutive iterations. The asymptotic boundary conditions Equation (17) were approximated by using $\eta_{\max} = 12$, $\theta(12) = 0 = \phi(12)$. Therefore, to transform the governing BVPs Equations (14)–(17) into the first order IVP, the new variables are defined as follows:

$$\begin{cases} f = y_1, \\ f' = y_2, \\ f'' = y_3, \\ f''' = y_3', \\ \theta = y_4, \\ \theta' = y_5, \\ \theta'' = y_5', \\ \phi = y_6, \\ \phi' = y_7, \\ \phi'' = y_7'. \end{cases} \tag{25}$$

Using Equation (18) into Equations (14)–(16) yields the following system of first order IVPs.

$$\begin{aligned}
y_1' &= y_2, \\
y_2' &= y_3, \\
y_3' &= \frac{{y_2}^2 + \frac{4}{3}\delta\lambda\gamma(1+2\gamma\eta){y_3}^3 - 2\gamma(1+\delta)y_{3,} + (M+K)y_2}{(1+\delta)(1+2\gamma\eta) - \delta\lambda(1+2\gamma\eta)^2 {y_3}^2}, \\
y_4' &= y_5, \\
y_5' &= \frac{\lambda_t y_1 y_2 y_5 - \frac{2\gamma y_5}{Pr} - y_1 y_5 - Nb(1+2\gamma\eta) y_5 y_7 - Nt(1+2\gamma\eta){y_5}^2 - Ec{y_3}^2\left[(1+\delta)(1+2\gamma\eta) - \frac{1}{3}\delta\lambda {y_3}^2\right] - Ec(M+K){y_2}^2}{\frac{(1+2\gamma\eta)}{Pr} - \lambda_t {y_1}^2}, \\
y_6' &= y_7, \\
y_7' &= Sc\lambda_c y_1 y_2 y_7 - 2\gamma y_7 - Sc y_1 y_7 - \frac{\mathrm{Nt}}{\mathrm{Nb}}\left[(1+2\gamma\eta)\frac{\lambda_t y_1 y_2 y_5 - \frac{2\gamma y_5}{Pr} - y_1 y_5 - Nb(1+2\gamma\eta) y_5 y_7 - Nt(1+2\gamma\eta){y_5}^2 - Ec{y_3}^2\left[(1+\delta)(1+2\gamma\eta) - \frac{1}{3}\delta\lambda {y_3}^2\right] - Ec(M+K){y_2}^2}{\frac{(1+2\gamma\eta)}{Pr} - \lambda_t {y_1}^2} + 2\gamma y_5\right].
\end{aligned} \tag{26}$$

In this case, the prime represents the derivative with respect to η. The transformed boundary conditions in Equation (17) are written as follows:

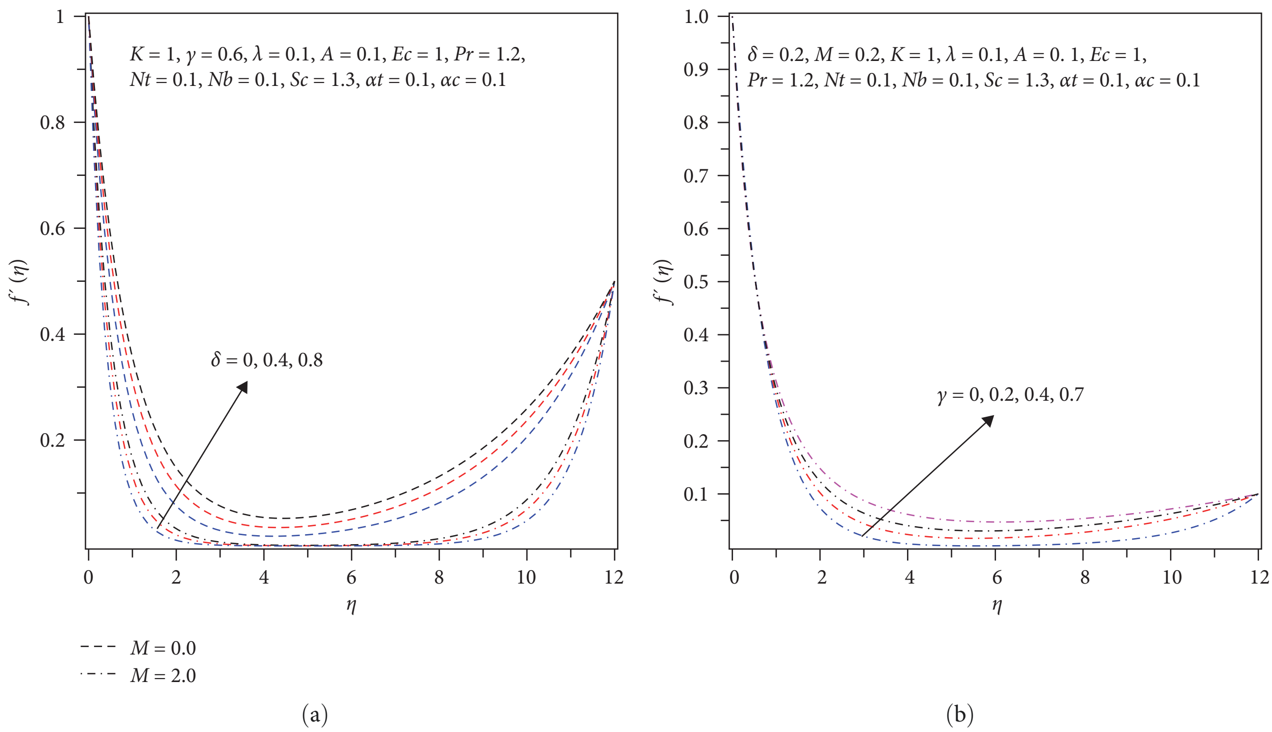

Figure 2: Velocity field (a) against δ, M and (b) against γ.

$$\begin{cases} y_1(0) = 0, \\ y_2(0) = 1, \\ y_3(0) = u_1, \\ y_4(0) = 1, \\ y_5(0) = u_2, \\ y_6(0) = u_3, \\ y_7(0) = -\dfrac{Nt}{Nb} u_2 \end{cases}, \tag{27}$$

where u_1, u_2, and u_3 are the suitable values of the initial guesses for $f``(0), \theta''(0)$ and $\phi(0)$, respectively. Besides, $y_1(\infty) \to A, y_2(\infty) \to 0, y_4(\infty) \to 0, y_6(\infty) \to 0$. The suitable values of the unknown initial conditions u_1, u_2, and u_3 are iteratively estimated until the solutions satisfy the boundary conditions at $\eta = \infty$ whereas R-K-45 is used to solve later on at $\eta = 0$.

4. Results and Discussions

4.1. Flow Field: Velocity Profile. Figure 2(a) is a double graph displaying the velocity profile against the magnetic parameter M and Eyring–Powell fluid parameter δ. It is noticed that the momentum boundary layer thickness and the velocity profile considerably increase as the size of δ increases because large value of δ indicates lower fluid viscosity so that it flows easily. Thus, as δ increases, the velocity profile also increases considerably. Therefore, velocity for the Eyring–Powell fluid exceeds that of viscous Newtonian fluid. Reverse to this, the momentum boundary layer thickness and the velocity profile decrease with increasing values of M. Physically, large value of magnetic parameter M corresponds to large resisting force that is called Lorentz resistance force, which dampens the fluid flow. Thus, as M increases, both the fluid velocity and the momentum boundary layer thickness decrease. Impact of the curvature parameter γ on fluid velocity is portrayed in Figure 2(b). Accordingly, both momentum boundary layer thickness and fluid velocity escalate when magnitude of γ rises. This can be justifiable because as γ increases the radius of the cylinder decreases which results in slender cylinder so that the contact surface area of the cylinder with the fluid decreases.

Thus, the surface of the cylinder accounts lower friction force on the movement of the fluid, which leads to an increase of fluid velocity.

Figures 3(a) and 3(b) illustrate the effects of the porous parameter K and the velocity ratio parameter A, respectively, on the velocity profile. Fluid velocity and thickness of the corresponding momentum boundary layer decrease as the value of the porous parameter K increases (Figure 3(a)). The argument behind this result is that bigger values of K physically indicates stronger resisting forces on the motion of the fluid that leads to the reduction of the fluid velocity. Hence, the inclusion of porous medium slows down the flow and a deceleration in the fluid velocity is observed Figure 3(b) also illustrates that both fluid velocity and thickness of the corresponding momentum boundary layer rise

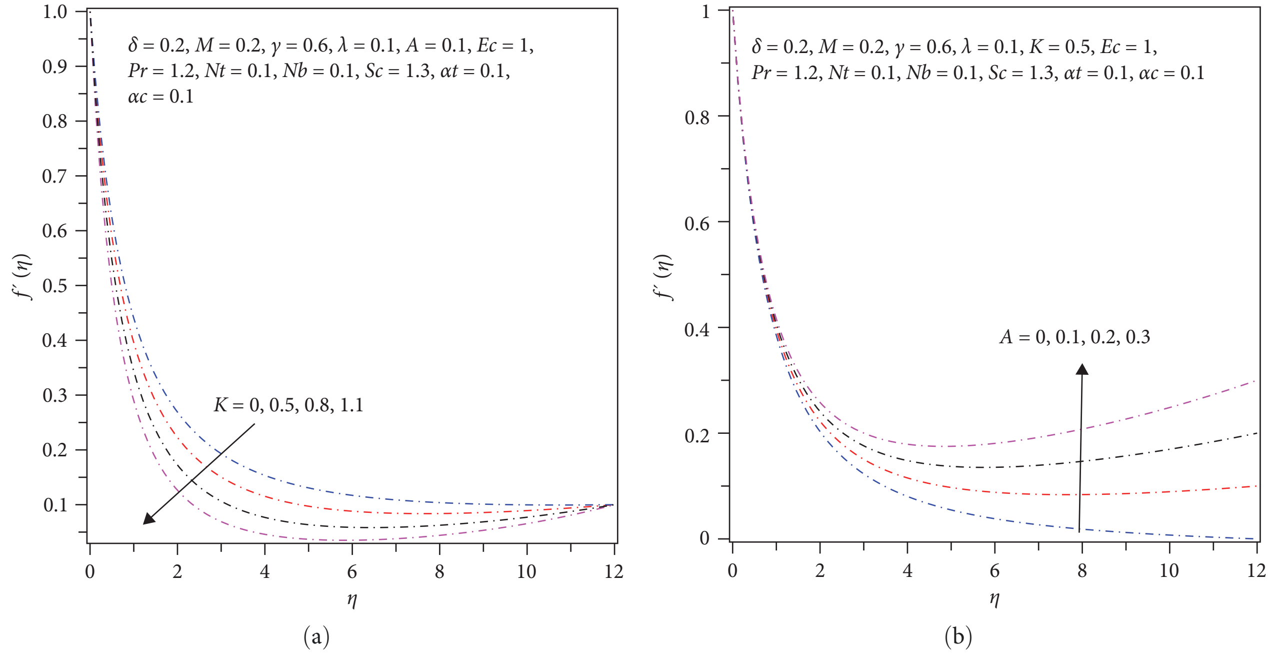

FIGURE 3: Velocity field (a) against K and (b) against A.

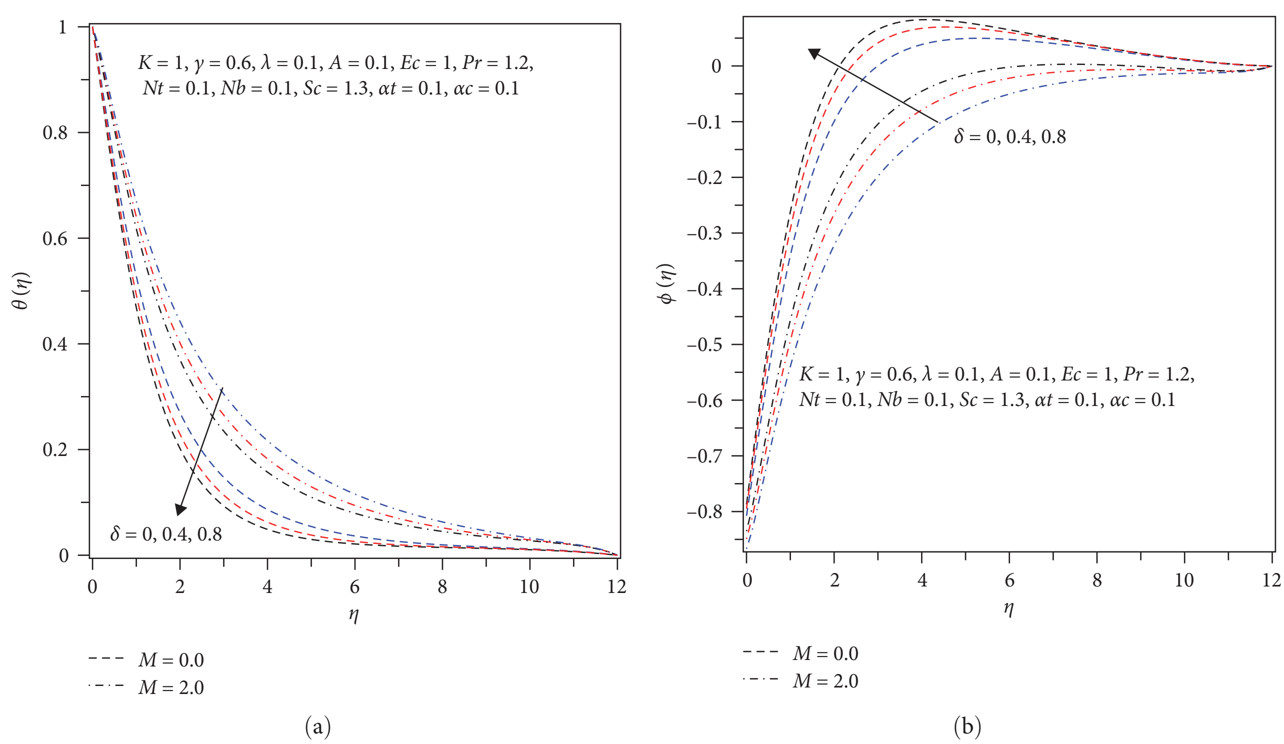

FIGURE 4: (a) Temperature field against δ, M and (b) concentration field against δ, M.

with increasing size of the velocity ratio parameter$A$ because physically, velocity ratio speeds up fluid motion that in turn boosts the velocity profile.

4.2. The Temperature and Concentration Profiles. Both the thickness of thermal boundary layer and fluid temperature enhance for larger values of the magnetic parameter$M$ as depicted in Figure 4(a). Physically, when M increases the Lorentzian resistant force increases and the friction between fluids layers which produces more heat leading to the rise of temperature profile. However, Figure 4(b) reveals the reverse situation for the nanoparticles concentration because of the

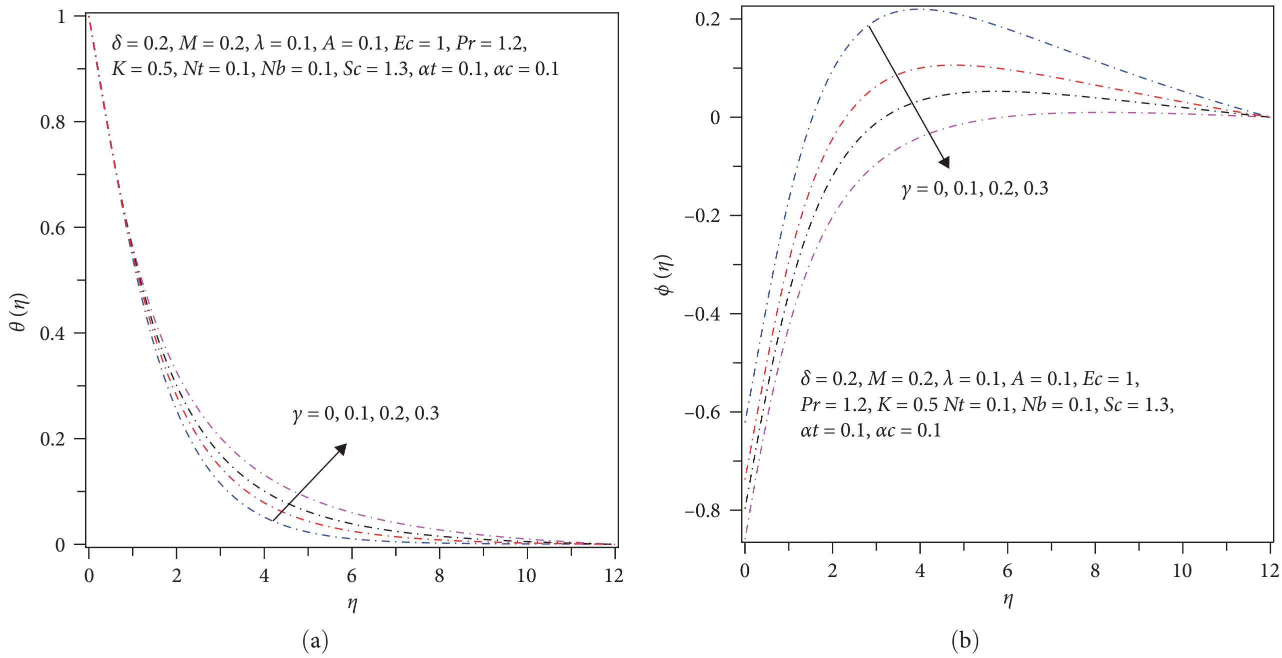

FIGURE 5: (a) Temperature field against γ and (b) concentration field against γ.

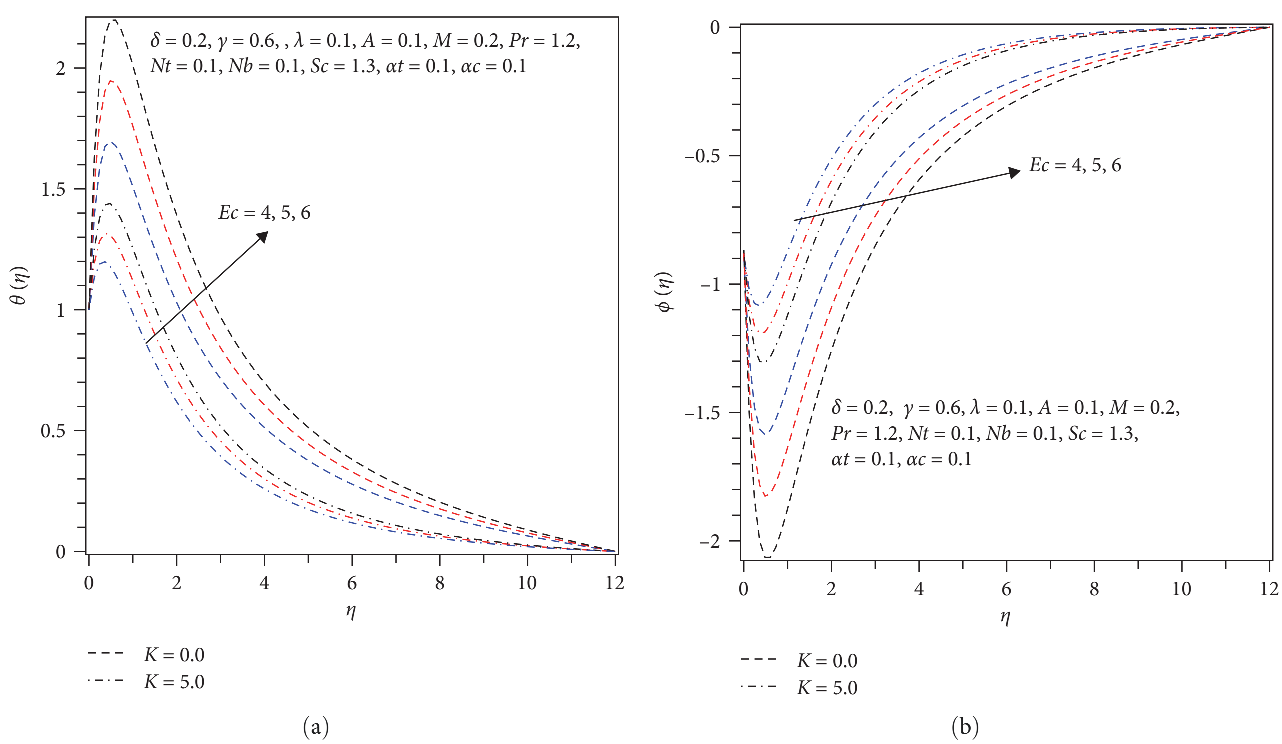

FIGURE 6: (a) Temperature field against Ec, K and (b) concentration field against Ec, K.

effect of cross diffusion. That is, small increase in temperature may cause small decrease in the nanoparticles concentration. Besides, as indicated in Figure 4(a), the thickness of thermal boundary layer and fluid temperature decline for bigger values of Eyring–Powell fluid parameter δ because bigger values in δ implies less viscous fluid which results in the lessening of friction among fluid particles and hence temperature distribution in the fluid falls down. Therefore, temperature of viscous Newtonian fluid is bigger as compared to temperature of non-Newtonian fluid past the porous cylinder that stretches. Although, Figure 4(b) demonstrates the reverse result for the case of the nanoparticles concentration.

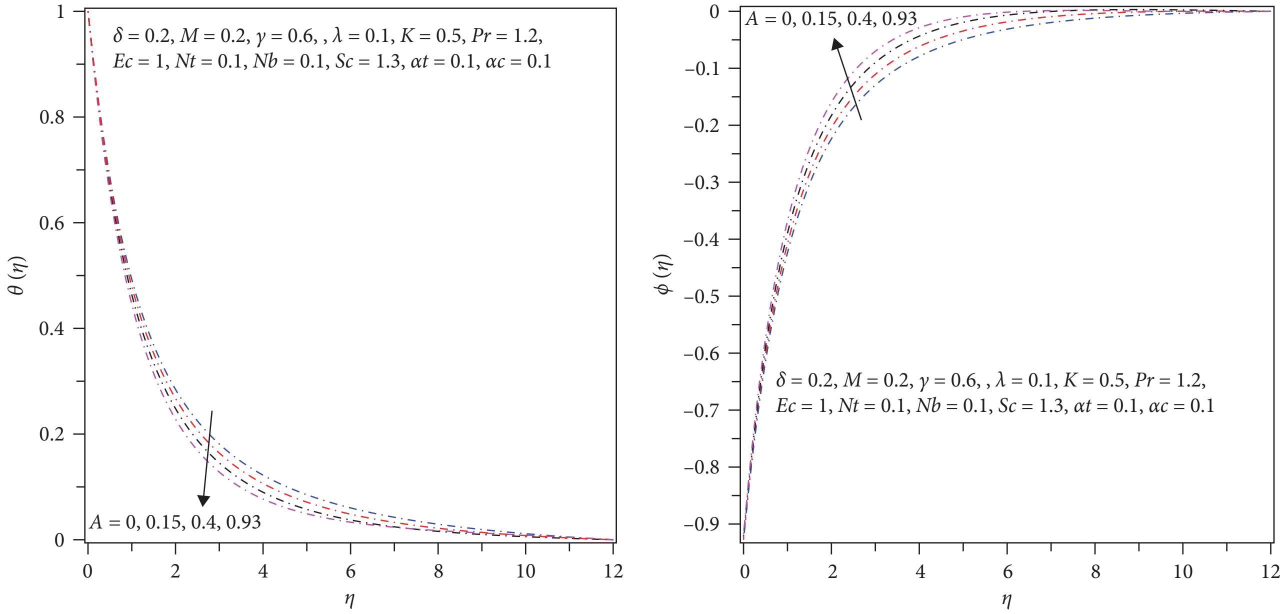

(a) (b)

Figure 7: (a) Temperature field against A and (b) concentration field against A.

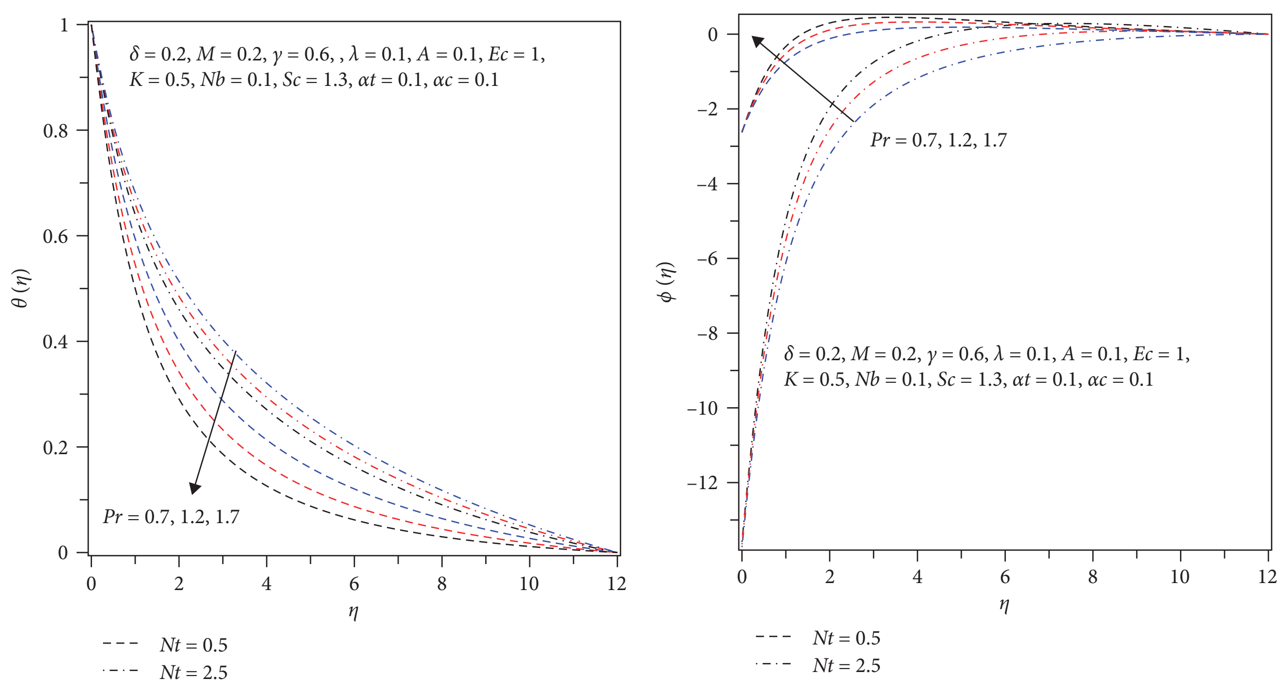

(a) (b)

Figure 8: (a) Temperature field against Pr, Nt and (b) concentration field against Pr, Nt.

Temperature profile is increasing significantly with the curvature parameter γ as exhibited in Figure 5(a). The physical interpretation can be, larger values of γ results in the decrement of radius of the cylinder resulting in the reduction of the friction force so that the velocity of the nanofluid rises as elaborated in Figure 2(b). Thus, the enhanced fluid velocity results in the escalation of the nanofluid kinetic energy, which in turn augments the heat energy of the nanofluid. Consequently, the nanofluid temperature increases as the curvature parameter γ increases. Additional insight into the effect of the same parameter on the concentration profile can be noticed from Figure 5(b). This figure reveals that the concentration profile significantly decreases with the increasing values of γ.

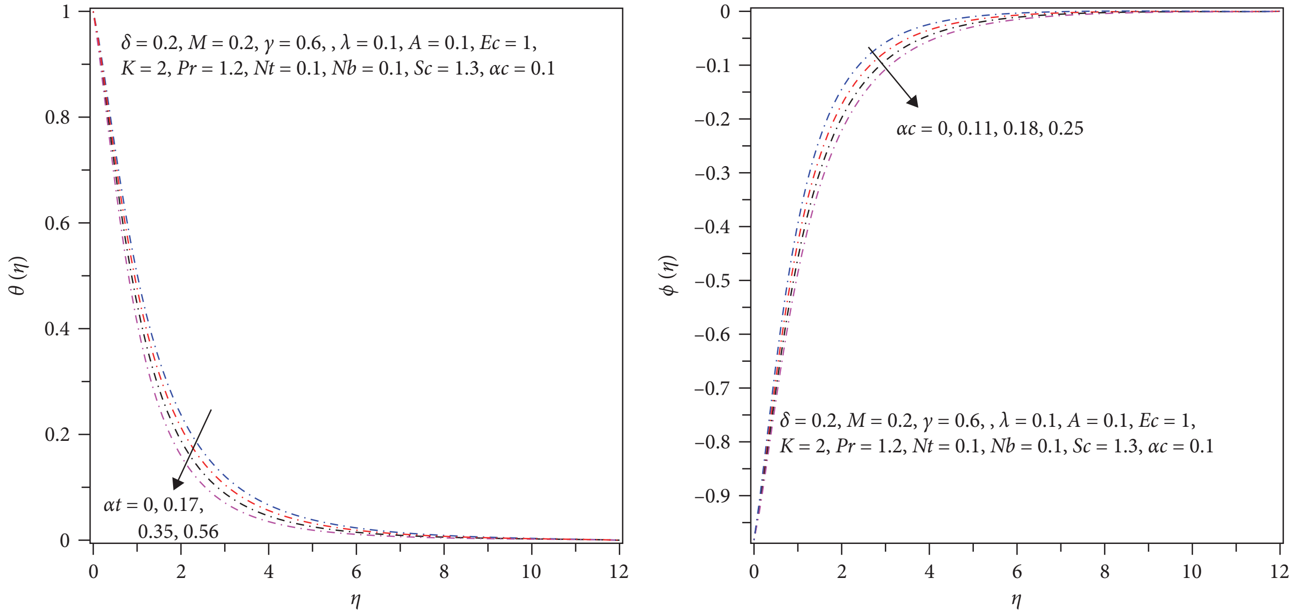

(a) (b)

Figure 9: (a) Temperature field against αt and (b) concentration field against αc.

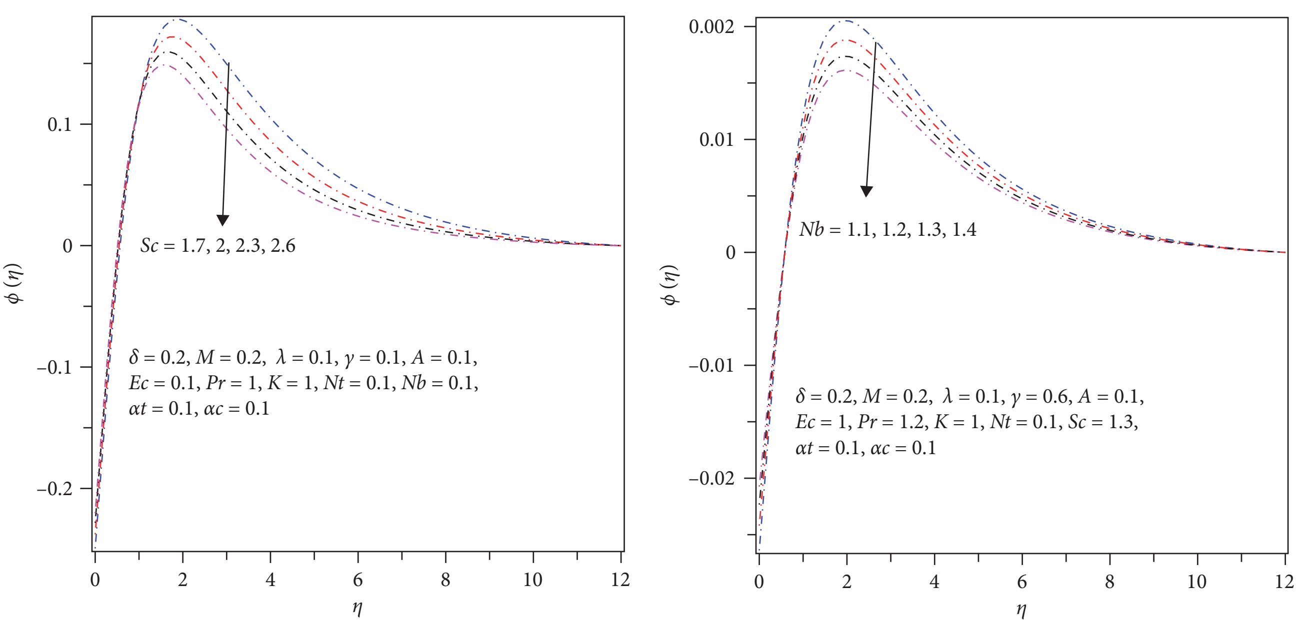

(a) (b)

Figure 10: Concentration field (a) against Sc and (b) against Nb.

As revealed in Figure 6(a), both the thickness of thermal boundary layer and fluid temperature escalate remarkably as the viscous dissipation factor (or Eckert number Ec) rises. The physical interpretation for this result is that the increment of Ec accumulates heat energy in the nanofluid because of heating caused by friction. Therefore, both temperature profile as well as the thickness of thermal boundary layer escalate as magnitude of Ec rises. The influence of the viscous dissipation parameter Ec on the concentration profile is reversed because of the cross-diffusion effect (Figure 6(b)). Figure 6(a) also displays the impact of the porous parameter K on the nanofluid temperature. Rising the values of K result in the lowering of the nanofluid temperature because the nanofluid velocity declines for larger values of K which in turn lowers the kinetic energy and thus, less heat energy is generated in the flow regime that leads to a low-nanofluid temperature.

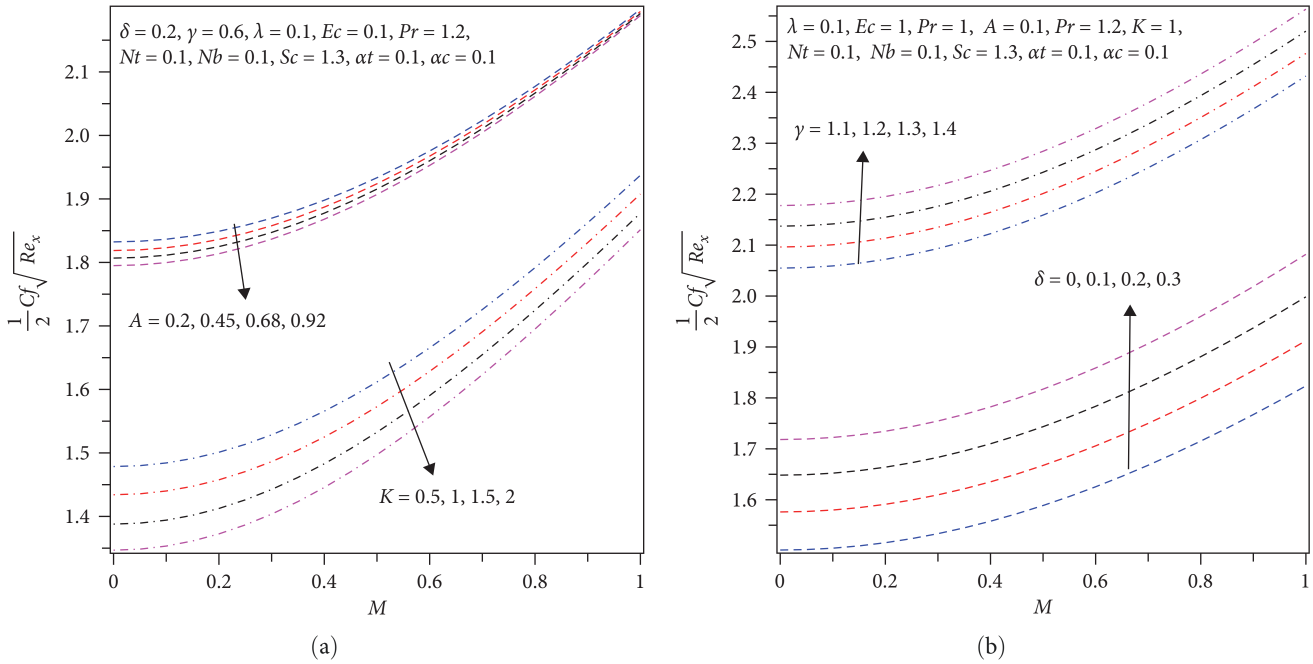

FIGURE 11: Skin friction coefficient with varying (a) A, K and (b) γ, δ.

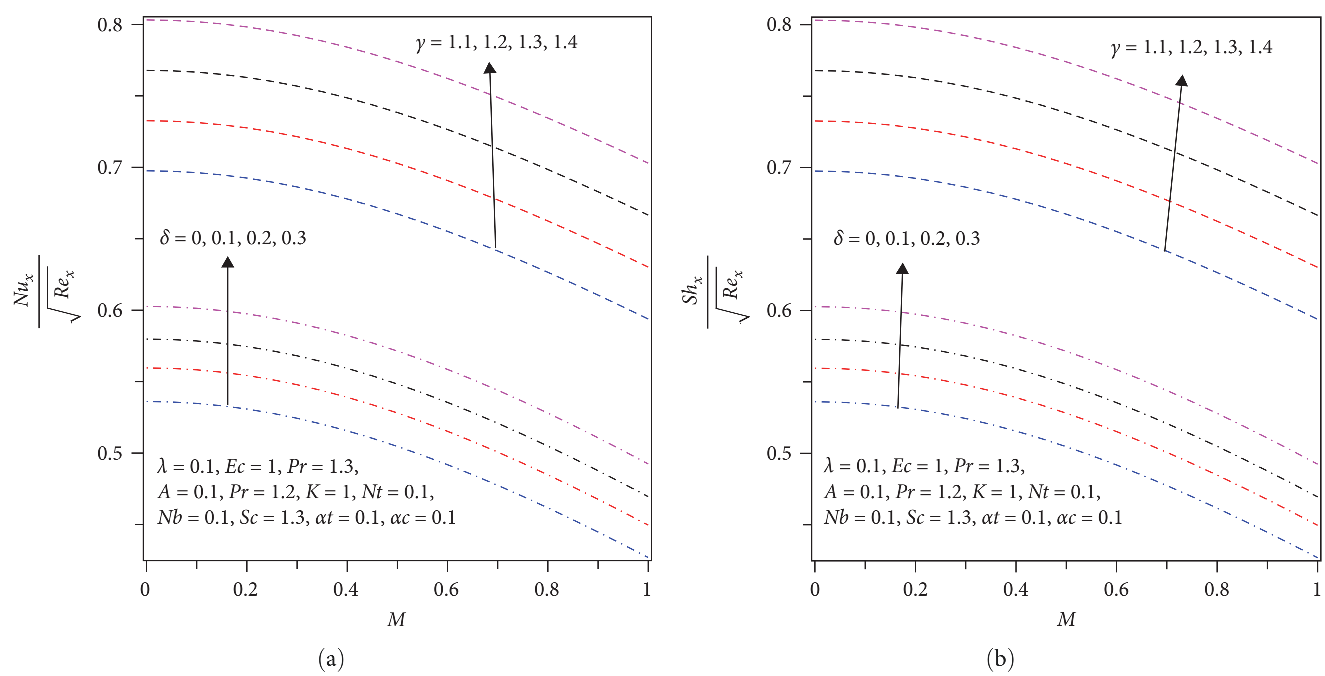

FIGURE 12: (a) Nusselt number with varying γ, δ and (b) Sherwood number with varying γ, δ.

Therefore, the porous medium reasonably and successfully managed nanofluid temperature as well as the overall thermal system in terms of system cooling, however, Figure 6(b) presented an opposite effect for the nanoparticles concentration.

Figure 7(a) illustrates that the temperature profile has shown a retarding pattern as the value of velocity ratio parameter A enhances whereas the concentration profile has indicated an opposite scenario as demonstrated in Figure 7(b).

The influences of thermophoresis Nt as well as Prandtl number Pr against the fluid temperature are demonstrated in Figure 8(a). It can be witnessed from the figure that the nanofluid temperature falls down strongly with rising Pr. Physically, large value of Pr represents a smaller thermal conductivity and hence there is a weak heat energy diffusion which results in a significant fall down of temperature profile. Besides, from the same figure, one can notice that

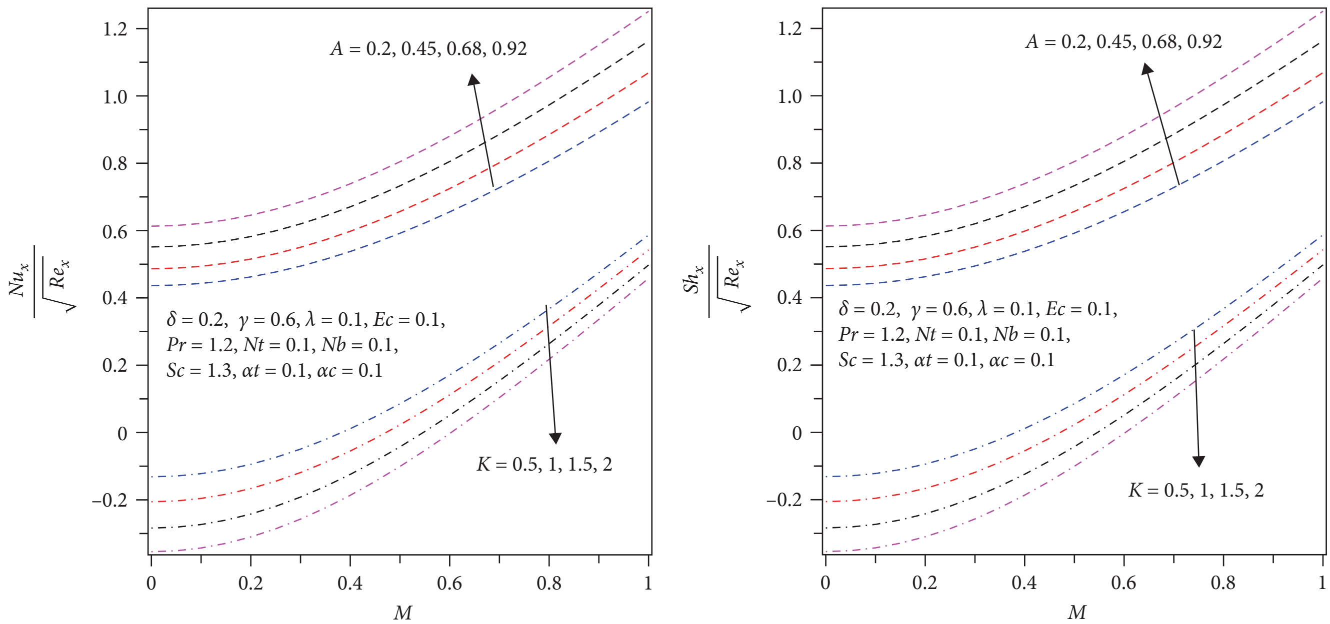

(a)

(b)

FIGURE 13: (a) Nusselt number with varying A, K and (b) Sherwood number with varying A, K.

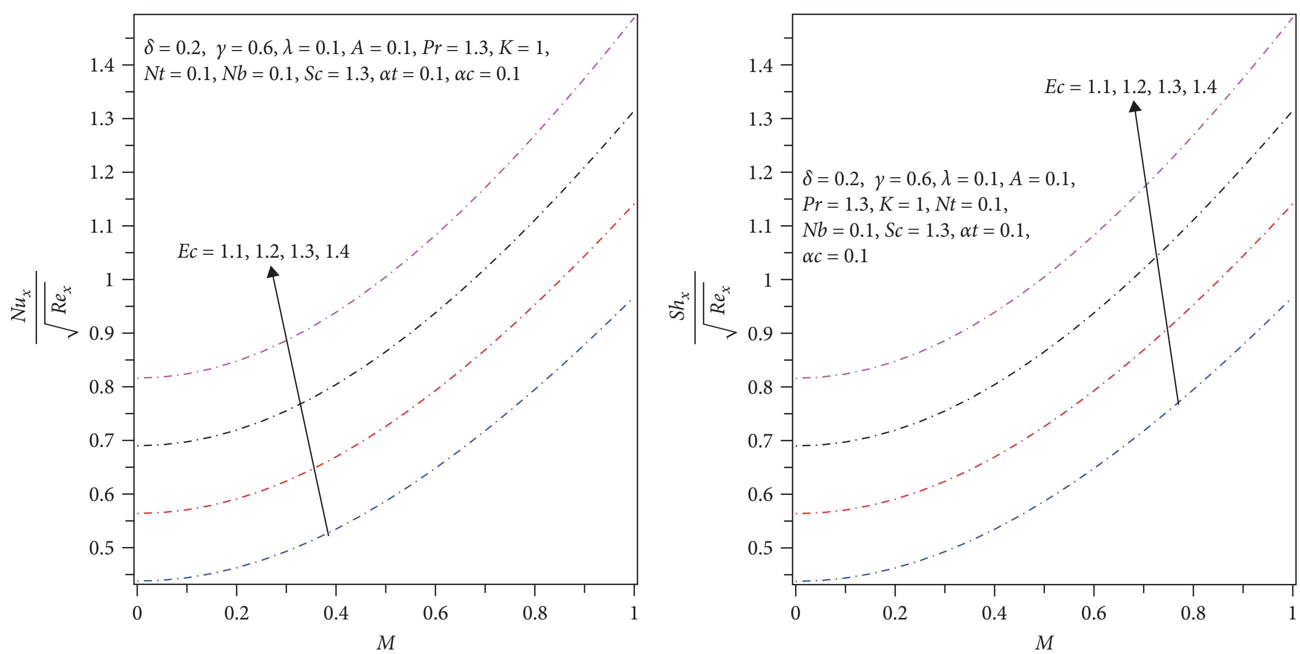

(a)

(b)

FIGURE 14: (a) Nusselt number with varying Ec and (b) Sherwood number with varying Ec.

nanofluid temperature enhances for increasing magnitudes of thermophoresis parameter Nt. In fact, thermophoresis is a process by which nanoparticles are moving out toward the cold region from the hot one and hence greater value of Nt corresponds to the tougher thermophoresis forces that favor the hot nanoparticles movement toward the cold fluid resulting in higher temperature distribution throughout the boundary layer flow. The influences of Pr and Nt on the concentration profile are also portrayed in Figure 8(b) where the scenarios are reversed because of the cross-diffusion effect.

Figure 9(a) portrayed the thickness of thermal boundary layer and temperature field against the Cattaneo–Christov time relaxation αt. Consequently, an increment of αt

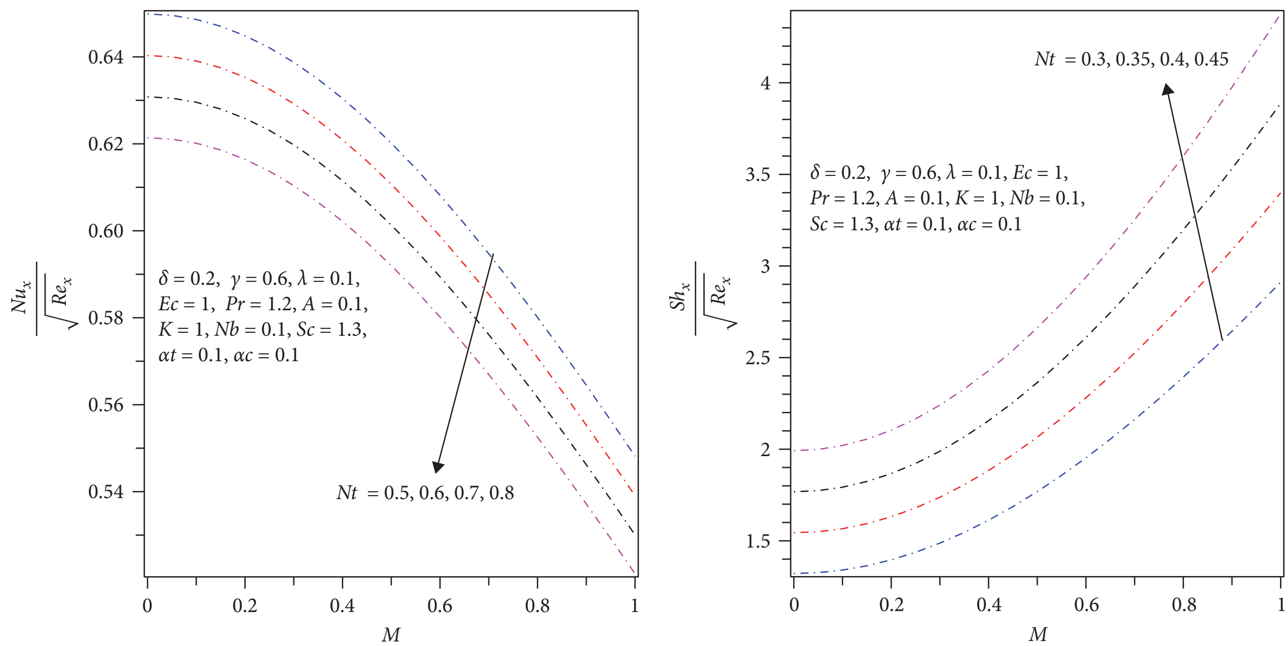

(a) (b)

Figure 15: (a) Nusselt number with varying Nt and (b) Sherwood number with varying Nt.

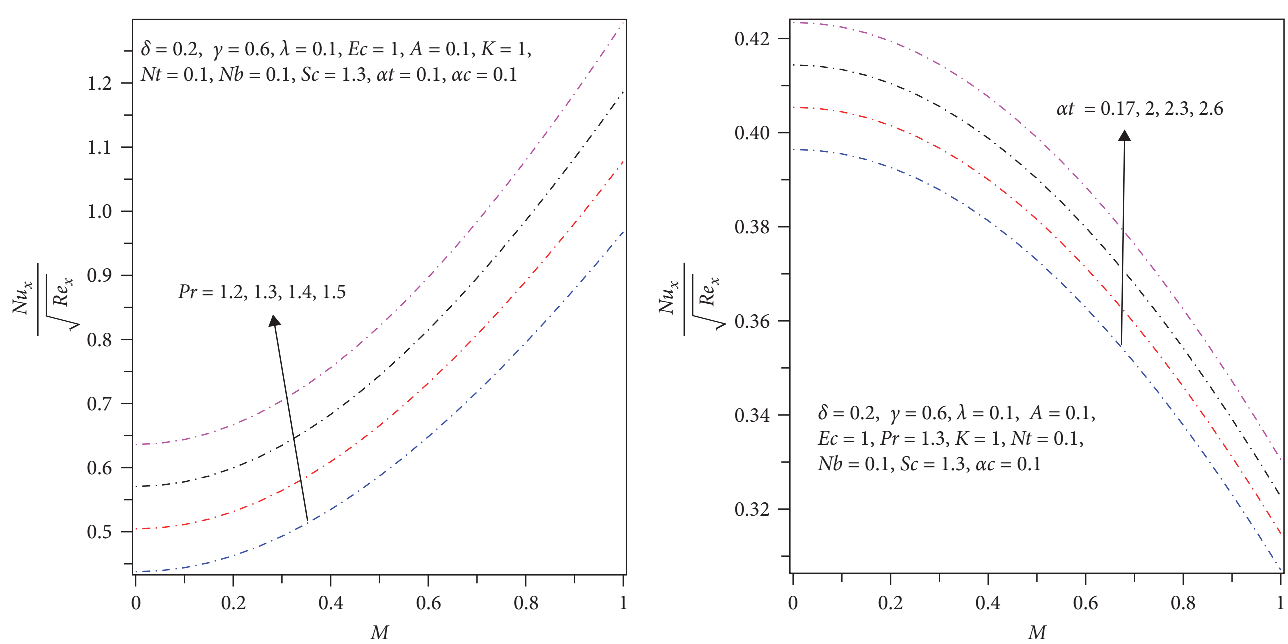

(a) (b)

Figure 16: Nusselt number with varying (a) Pr and (b) αt.

indicates a decreasing pattern for the temperature profile. In physical sense, as αt increases, the nanofluid acquires additional more periods for transferring heat energy into the surrounding and thus, nanofluid temperature falls down. Therefore, a falling down of nanofluid temperature is observed when a magnitude of αt rises. Indeed, for the mixed convection of nanofluid over a porous cylinder the Cattaneo–Christov model produces more heat when compared to the heat conduction laws of Fourier ($\alpha t = 0$). Therefore, the Cattaneo–Christov heat flux model is favorable in regulating large heat flux situations when compared to the heat conduction laws of Fourier. Similarly, Figure 9(b) reveals variation of the

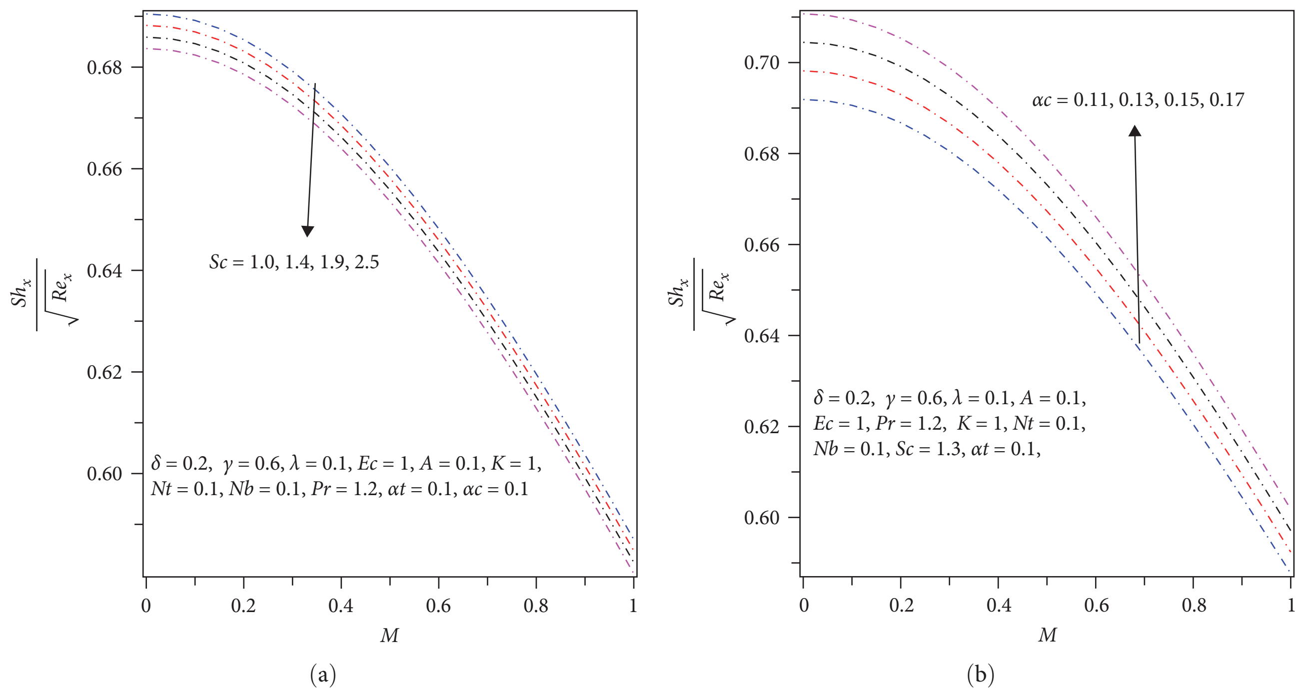

FIGURE 17: Sherwood number with varying (a) Sc and (b) αc.

concentration profile with assorted values of solutal relaxation time parameter αc. The nanoparticle concentration shows a decreasing behavior with the escalating values of αc

Figure 10(a) illustrates that the concentration profile drops in response to a rise in the Schmidt number Sc. Physically, big value of Sc indicates a small mass diffusion in the flow regime and thus nanoparticles concentration drops when a size of Sc increases. Moreover, Figure 10(b) displayed impacts of Brownian motion factor Nb against nanoparticles concentration. Both the thickness of concentration boundary layer and nanoparticles concentration decline with the escalating sizes of Nb. This is the case since large value of Nb shows an enhanced nanoparticles collision as well as random movements that in turn declines the nanoparticles concentration throughout flow regime.

4.3. Skin Friction Coefficient, Nusselt Number, and Sherwood Number. Figures 11(a) and 11(b) are presented to visualize the effects of velocity ratio parameter A, porous parameter K, curvature parameterγ, and Eyring–Powell fluid parameterδ on coefficient of skin friction C_f where M (magnetic parameter) is used for scaling the horizontal axis. From Figure 11(a) it is clearly examined that C_f gets cut down with increasing values of K and A. However, C_f gets rise up for increasing values of γ and δ as elucidated in Figure 11(b).

Escalating the magnitudes of γ (curvature parameter) as well as δ (Eyring–Powell fluid parameter) results in the enhancement of both Nu (Nusselt number) and Sh (Sherwood number) as illustrated in Figures 12(a) and 12(b), respectively, with scaled values of the magnetic parameter M. Furthermore, Nu and Sh are rising with the velocity ratio parameter A but both are falling with the porous parameter K as displayed in Figures 13(a) and 13(b), respectively. The Eckert number Ec is directly related to both Nu and Sh (Figures 14(a) and 14(b)). The thermophoresis parameter Nt has revealed a retarding effect on Nu but a rising effect on Sh as demonstrated in Figures 15(a) and 15(b), respectively. In addition, Figures 16(a) and 16(b) displayed that the Nusselt number Nu increases with the increasing values of Prandtl number Pr and thermal relaxation time αt. Furthermore, Schmidt number Sc indicates a retarding influence on Sh while solutal relaxation time αc shows a rising impact on Sh as portrayed in Figures 17(a) and 17(b), respectively.

In order to validate the accuracy of the current numerical technique, comparison is done in the case of the skin friction coefficients for the present results with some limited conditions against that of already available literatures. Thus, an excellent as well as a sound agreement is attained up on comparing with Ibrahim and Hindebu [5] and Layek et al. [6] as witnessed in Table 1.

TABLE 1: Comparison of $-1/2C_f\sqrt{Re_x}$ in the case of varying λ values for $Pr=1.7, Sc=2, \delta=0.2, Nt=0.1=Nb,$ and $M=\gamma=\alpha t=\alpha c=K=Ec=0$.

	$-\frac{1}{2}C_f\sqrt{Re_x}$		
λ	Ibrahim and Hindebu [5]	Layek et al. [6]	Present results
0.1	1.0940	1.0940	1.0940
0.2	1.0925	1.0924	1.0925
0.3	1.0909	1.0909	1.0909
0.4	1.0894	1.0894	1.0894
0.5	1.0878	1.0878	1.0878
0.6	1.0863	1.0862	1.0863
0.7	1.0847	1.0847	1.0847

5. Conclusions

The current study aims to scrutinize the flow dynamics of Eyring–Powell nanofluid on porous stretching cylinder under the effects of magnetic field and viscous dissipation by employing Cattaneo–Christov theory. In order to study impacts of thermophoretic force and Brownian motion, the two-phase (Buongiorno) model is considered. As a consequence, very nonlinear PDEs that govern flow problem were formulated, transformed into ODEs via relevant similarity variables, as well as tackled by utilizing R-K-45 integration scheme along with the shooting technique in the MATLAB R2018a software. Hence, the effects of pertinent embedded thermo-physical parameters on velocity, temperature, and concentration profiles as well as on the skin friction coefficient, the wall heat transfer and mass transfer rates are investigated and displayed through graphs. Based on the results and discussions made under the previous section, the major findings of the current investigation are summarized as follows:

(i) The Eyring–Powell fluid parameter δ, curvature parameter γ, and velocity ratio parameter A have a propensity to raise the momentum boundary layer thickness and the velocity profile.

(ii) The thickness of thermal boundary layer as well as temperature profile show rising trend as the magnitudes of M (magnetic parameter), γ (curvature parameter), viscous dissipation factor (or Eckert number Ec), and thermophoresis parameter Nt enhance.

(iii) The Eyring–Powell fluid parameter δ, Prandtl number Pr, porous parameter K, velocity ratio parameter A, and thermal relaxation time αt indicate a retarding effect on the temperature profile and thermal boundary layer thickness.

(iv) The concentration profile gets fall down with rising values of the magnetic parameter M, curvature parameter γ, Eckert number Ec and thermophoresis parameter Nt, Brownian motion parameter Nb, Schmidt number Sc, and solutal relaxation time αc.

(v) The skin friction coefficient C_f escalates for increasing values of the Eyring–Powell fluid parameter δ, M (magnetic parameter), and γ (curvature parameter) while it falls down when both K (porous parameter) as well as A (velocity ratio parameter) rise.

(vi) The curvature parameter γ, magnetic parameter M, Eyring–Powell fluid parameter δ, velocity ratio parameter A, and Eckert number Ec revealed an escalating pattern against both Nusselt number Nu and Sherwood number Sh while both get cut down with the porous parameter K.

(vii) The Nusselt number Nu increases with increasing values of Prandtl number Pr and thermal relaxation time αt.

(viii) The Sherwood number Sh indicates a decreasing pattern with rising sizes for Sc (Schmidt number) while αc (solutal relaxation time) shows an increasing effects on Sherwood number Sh.

Nomenclature

A: Velocity ratio parameter
B_0: Uniform magnetic field strength
C: Nanoparticles concentration
C_f: Coefficient of skin friction
C_w: Concentration at the surface of the cylinder
C_∞: Concentration at the free stream
D_B: Brownian diffusion coefficient
D_T: Thermal diffusion coefficient
Ec: Eckert number
f: Dimensionless stream function
K: Porous parameter
k: Thermal conductivity of fluid
M: Dimensionless magnetic parameter
Nb: Brownian motion parameter
Nt: Thermophoresis parameter
Nu: The Nusselt number
Pr: The Prandtl number
Sc: The Schmidt number
Sh: The Sherwood number
T: Nanofluid temperature
T_w: Surface temperature
T_∞: Free stream temperature
u_w: Stretching velocity of the cylinder
U_∞: Velocity at the free stream
αt: Relaxation time parameter in the case of temperature
αc: Relaxation time parameter in the case of concentration
δ: Eyring-fluid parameter
γ: Dimensionless stretching parameter
Ψ: Dimensional stream function
H: Similarity variable
θ: Dimensionless nanofluid temperature
Φ: Dimensionless nanoparticles concentration.

Data Availability

No underlying data were collected or produced in this study.

Conflicts of Interest

The author declares that there is no conflicts of interest.

References

[1] U. Khan, A. Zaib, S. A. Bakar, A. Ishak, D. Baleanu, and E. M. Sherif, "Computational simulation of cross-flow of Williamson fluid over a porous shrinking/stretching surface comprising hybrid nanofluid and thermal radiation," *AIMS Mathematics*, vol. 7, no. 4, pp. 6489–6515, 2022.

[2] E. O. Fatunmbi and A. T. Adeosun, "Nonlinear radiative Eyring–Powell nanofluid flow along a vertical Riga plate with exponential varying viscosity and chemical reaction," *International Communications in Heat and Mass Transfer*, vol. 119, pp. 1–10, 2020.

[3] K. Al-Khaled, S. U. Khan, and I. Khan, "Chemically reactive bioconvection flow of tangent hyperbolic nanoliquid with gyrotactic microorganisms and nonlinear thermal radiation," *Heliyon*, vol. 6, no. 1, Article ID e03117, 2020.

[4] R. E. Powell and H. Eyring, "Mechanism for relaxation theory of viscosity," *Nature*, vol. 154, no. 3909, pp. 427-428, 1944.
[5] W. Ibrahim and B. Hindebu, "Magnetohydrodynamic boundary layer flow of Eyring–Powell nanofluid past stretching cylinder with Cattaneo–Christov heat flux model," *Nonlinear Eng*, vol. 8, no. 1, pp. 1–15, 2018.
[6] G. C. Layek, B. Mandal, and K. Bhattacharyya, "Dufour and soret effects on unsteady heat and mass transfer for Powell–Eyring fluid flow over an expanding permeable sheet," *Journal of Applied and Computational Mechanics*, vol. 6, no. 4, pp. 985–998, 2020.
[7] I. Jabeen, M. Farooq, M. Rizwan, R. Ullah, and S. Ahmad, "Analysis of nonlinear stratified convective flow of Powell–Eyring fluid: application of modern diffusion," *Advances in Mechanical Engineering*, vol. 12, no. 10, pp. 1–10, 2020.
[8] F. Salah, "Chemical reaction and generalized heat flux model for Powell–Eyring model with radiation effects," *International Journal of Mathematics and Mathematical Sciences*, vol. 2022, Article ID 4076426, 11 pages, 2022.
[9] S. Akram, M. Athar, K. Saeed, and M. Y. Umair, "Double-diffusivity convection on powelleyring nanofluids in non-uniform inclined channel under the impact of peristaltic propulsion and induced magnetic field," *European Physical Journal Plus*, vol. 136, pp. 478–494, 2021.
[10] T. Naseem, I. Bibi, A. Shahzad, and M. Munir, "Analysis of heat transport in a Powell–Eyring fluid with radiation and joule heating effects via a similarity transformation," *Fluid Dynamics & Materials Processing*, vol. 19, no. 3, pp. 663–677, 2023.
[11] A. M. Alqahtani, M. O. Sidi, M. R. Khan, M. A. Elkotb, E. Tag-Eldin, and A. M. Galal amd, "Transport properties of two-dimensional dissipative flow of hybrid nanofluid with Joule heating and thermal radiation," *Scientific Reports*, vol. 12, pp. 1–16, Article ID 19374, 2022.
[12] S. U. S. Choi, "Enhancing thermal conductivity of fluids with nanoparticles," *ASME International Mechanical Engineering*, vol. 66, pp. 99–105, 1995.
[13] O. A. Abo-zaid, R. A. Mohamed, F. M. Hady, and A. Mahdy, "MHD Powell–Eyring dusty nanofluid flow due to stretching surface with heat flux boundary condition," *Journal of the Egyptian Mathematical Society*, vol. 29, no. 1, pp. 1–14, 2021.
[14] M. O. Lawal, K. B. Kasali, H. A. Ogunseye, M. O. Oni, Y. O. Tijani, and Y. T. Lawal, "On the mathematical model of Eyring–Powell nanofluid flow with non-linear radiation, variable thermal conductivity and viscosity," *Partial Differential Equations in Applied Mathematics*, vol. 5, Article ID 100318, 2022.
[15] A. Nazash, W. A. Khan, A. Hobiny, M. Azam, M. Waqas, and M. Irfan, "Numerical analysis for thermal performance of modified Eyring–Powell nanofluid flow subject to activation energy and bioconvection dynamics," *Case Studies in Thermal Engineering*, vol. 39, pp. 1–12, 2022.
[16] R. A. Mohamed, S. M. Abo-Dahab, and M. S. Soliman, "Effects of nonlinear thermal radiation and heat generation/absorption on magnetohydrodynamic (MHD) carreau nanofluid flow on a nonlinear stretching surface through a porous medium," *Journal of Nanofluids*, vol. 11, no. 6, pp. 845–856, 2022.
[17] A. Shahzad, F. Liaqat, Z. Ellahi, M. Sohail, M. Ayub, and M. R. Ali, "Thin film flow and heat transfer of Cu-nanofluids with slip and convective boundary condition over a stretching sheet," *Scientific Reports*, vol. 12, no. 1, Article ID 14254, 2022.
[18] A. Ali, S. Murtaza, M. Memon, K. Bhatti, M. Haque, and M. Ali, "Simulation of thermal decomposition of calcium oxide in water with different activation energy and the high reynolds number," *Complexity*, vol. 2022, Article ID 3950242, 21 pages, 2022.
[19] M. Abdul Basit, M. Imran, S. A. Khan, A. Alhushaybari, R. Sadat, and M. R. Ali, "Partial differential equations modeling of bio-convective sutterby nanofluid flow through paraboloid surface," *Scientific Reports*, vol. 13, no. 1, 2023.
[20] U. Nazir, M. Sohail, P. Kumam et al., "Thermal and solute aspects among two viscosity models in synovial fluid inserting suspension of tri and hybrid nanomaterial using finite element procedure," *Arabian Journal of Chemistry*, vol. 12, 2022.
[21] F. Umar Farooq, W. Hassan, S. A. Musaad et al., "Modeling and computational framework of radiative hybrid nanofluid configured by a stretching surface subject to entropy generation: using Keller box scheme," *Scientific Reports*, vol. 16, no. 4, Article ID 104628, 2023.
[22] Y. Mahmoudi, K. Hooman, and K. Vafai, *Convective Heat Transfer in Porous Media*, Taylor & Francis Group. CRC Press, 2020.
[23] A. A. A. A. Al-Rashed, G. A. Sheikhzadeh, A. Aghaei, F. Monfared, A. Shahsavar, and M. Afrand, "Effect of a porous medium on flow and mixed convection heat transfer of nanofluids with variable properties in a trapezoidal enclosure," *Journal of Thermal Analysis and Calorimetry*, vol. 139, no. 1, pp. 741–754, 2020.
[24] M. Muthtamilselvan and S. Sureshkumar, "A tilted lorentz force effect on porous media filled with nanofluid," *Journal of Theoretical and Applied Mechanics*, vol. 48, no. 2, pp. 50–71, 2018.
[25] S. Whitaker, "Flow in porous media I: a theoretical derivation of Darcy's law," *Transport in Porous Media*, vol. 1, no. 1, pp. 3–25, 1986.
[26] M. Tasmin, P. Nag, Z. T. Hoque, and M. M. Molla, "Non-Newtonian effect on heat transfer and entropy generation of natural convection nanofluid flow inside a vertical wavy porous cavity," *SN Applied Sciences*, vol. 3, no. 3, 2021.
[27] N. Shirani and D. Toghraie, "Numerical investigation of transient mixed convection of nanofluid in a cavity with non-Darcy porous inner block and rotating cylinders with harmonic motion," *Scientific Reports*, vol. 11, no. 1, Article ID 17281, 2021.
[28] M. Bilal, I. Khan, T. Gul et al., "Darcy forchheimer hybrid nano fluid flow with mixed convection past an inclined cylinder," *Computers Materials & Continua(CMC)*, vol. 66, no. 2, pp. 2026–2039, 2021.
[29] A. K. Verma, S. Rajput, K. Bhattacharyya, A. J. Chamkha, and D. Yadav, "Comparison between graphene–water and graphene oxide–water nanofluid flows over exponential shrinking sheet in porous medium: dual solutions and stability analysis," *Chemical Engineering Journal Advances*, vol. 12, pp. 1–10, 2022.
[30] B. Shruti, M. M. Alam, A. Parkash, and S. Dhinakaran, "Darcy number influence on natural convection around porous cylinders in an enclosure using Darcy–BrinkmanForchheimer model: LBM study," *Case Studies in Thermal Engineering*, vol. 45, Article ID 102907, 2023.
[31] A. M. Rashad, M. A. Nafe, and D. A. Eisa, "Heat generation and thermal radiation impacts on flow of magnetic Eyring–Powell hybrid nanofluid in a porous medium," *Arabian Journal for Science and Engineering*, vol. 48, pp. 939–952, 2023.

[32] M. A. Aslam, H. Yao, M. K. Al Mesfer et al., "Finite element modeling of dual convection in a Y shaped porous cavity containing viscus fluid," *Frontiers in Physics*, vol. 11, pp. 1–13, 2023.

[33] S. R. R. Reddy, P. Bala Anki Reddy, and A. M. Rashad, "Activation energy impact on chemically reacting Eyring–Powell nanofluid flow over a stretching cylinder," *Arabian Journal for Science and Engineering*, vol. 45, no. 7, pp. 5227–5242, 2020.

[34] M. Ramza, Z. Shah, P. Kumam, W. Khan, W. Watthayu, and W. Kumam, "Bidirectional flow of MHD nanofluid with hall current and Cattaneo–Christove heat flux toward the stretching surface," *PLoS One*, vol. 17, no. 4, Article ID e0264208, 2022.

[35] N. Abbas, W. Shatanawi, A. Taqi, and M. Shatnawi, "Transportation of nanomaterial Maxwell fluid flow with thermal slip under the effect of Soret–Dufour and second-order slips: nonlinear stretching," *Scientific Reports*, vol. 13, Article ID 2182, 2023.

[36] C. H. N. Raju, C. S. Reddy, M. A. Alyami et al., "MHD Eyring–Powell nanofluid flow across a wedge with convective and thermal radiation," *Frontiers in Energy Research*, vol. 10, Article ID 1021491, 2022.

[37] M. S. Arif, M. Jhangir, Y. Nawaz, I. Abbas, M. Abodayeh, and A. Ejaz, "Numerical study for magnetohydrodynamic (MHD) unsteady maxwell nanofluid flow impinging on heated stretching sheet," *Computer Modeling in Engineering & Sciences*, vol. 133, no. 2, pp. 303–325, 2022.

[38] M. D. Shamshuddin, F. Mebarek-Oudina, S. O. Salawu, and A. Shafiq, "Thermophoretic movement transport of reactive casson nanofluid on riga plate surface with nonlinear thermal radiation and uneven heat sink/source," *Journal of Nanofluids*, vol. 11, pp. 833–844, 2022.

[39] S. Gupta, D. Kumar, and J. Singh, "Analytical study for MHD flow of Williamson nanofluid with the effects of variable thickness, nonlinear thermal radiation and improved Fourier's and Fick's Laws," *SN Applied Sciences*, vol. 2, no. 3, pp. 1–12, 2020.

[40] A. H. Majeed, R. Mahmood, H. Shahzad et al., "Heat and mass transfer characteristics in MHD Casson fluid flow over a cylinder in a wavy channel: higher-order FEM computations," *Case Studies in Thermal Engineering*, vol. 42, pp. 102730–102746, 2023.

[41] M. Mughees, M. Sajid, M. N. Sadiq, H. Shahzad, and N. Ali, "Blade coating analysis of carreau fluid model with magnetohydrodynamics and slip effects," *Journal of Plastic Film & Sheeting*, vol. 39, no. 2, pp. 151–173, 2023.

[42] I. S. Chuhan, J. Li, Z. Guo, H. Shahzad, and M. Yaqub, "Entropy optimization of MHD non-Newtonian fluid in a wavy enclosure with double diffusive natural convection," *Numerical Heat Transfer, Part A: Applications*, pp. 1–21, 2023.

[43] H. Shahzad, Q. U. Ain, A. A. Pasha et al., "Double-diffusive natural convection energy transfer in magnetically influenced Casson fluid flow in trapezoidal enclosure with fillets," *International Communications in Heat and Mass Transfer*, vol. 137, pp. 106236–106253, 2022.

[44] A. H. Majeed, A. Zeeshan, and M. Jawad, "Double stratification impact on radiative MHD flow of nanofluid toward a stretchable cylinder under thermophoresis and Brownian motion with multiple slip," *International Journal of Modern Physics B*, vol. 37, no. 24, Article ID 2350232, 2023.

[45] J. Akram, A. Zeeshan, M. S. Alhodaly, and M. Marin, "Evaluation of Magnetohydrodynamics of Natural Convective Heat Flow over Circular Cylinder Saturated by Nanofluid with Thermal Radiation and Heat Generation Effects," *Mathematics*, vol. 10, no. 11, Article ID 1858, 2022.

[46] A. Zeeshan, O. U. Mehmood, F. Mabood, and F. Alzahrani, "Numerical analysis of hydromagnetic transport of casson nanofluid over permeable linearly stretched cylinder with Arrhenius activation energy," *International Communications in Heat and Mass Transfer*, vol. 130, Article ID 105736, 2022.

[47] G. Narender, K. Govardhan, and G. Sreedhar Sarma, "Numerical study of radiative magnetohydrodynamics viscous nanofluid due to convective stretching sheet with the chemical reaction effect," *Iraqi Journal of Science*, vol. 61, no. 7, pp. 1733–1744, 2020.

[48] W. Abbas and A. M. Megahed, "Powell–Eyring fluid flow over a stratified sheet through porous medium with thermal radiation and viscous dissipation," *AIMS Mathematics*, vol. 6, no. 12, pp. 13464–13479, 2021.

[49] A. Olkha and A. Dadheech, "Unsteady magnetohydrodynamics slip flow of Powell–Eyring fluid with microorganisms over an inclined permeable stretching sheet," *Journal of Nanofluids*, vol. 10, no. 1, pp. 128–145, 2021.

[50] A. Mishra and M. Kumar, "Velocity and thermal slip effects on MHD nanofluid flow past a stretching cylinder with viscous dissipation and Joule heating," *SN Applied Sciences*, vol. 2, no. 8, Article ID 1350, 2020.

[51] K. R. Babu, G. Narender, and K. Govardhan, "MHD flow of an Eyring–Powell fluid with the effect of thermal radiation, Joule heating and viscous dissipation," *Advances in Mathematics: Scientific Journal*, vol. 9, no. 11, pp. 9259–9271, 2020.

[52] K. Ramesh, D. Patidar, and O. Ojjela, "Entropy generation analysis of free convection radiative MHD Eyring–Powell fluid flow between porous parallel plates with soret and dufour effects," *Heat Transfer*, vol. 50, no. 7, pp. 6935–6954, 2021.

[53] S. Sadighi, H. Afshar, H. Ahmadi Danesh Ashtiani, and M. Jabbari, "MHD flow and conductive heat transfer on a permeable stretching cylinder: benchmark solutions," *Case Studies in Thermal Engineering*, vol. 44, Article ID 102886, 2023.

[54] S. Jayanthi and H. Niranjan, "Effects of Joule heating, viscous dissipation, and activation energy on nanofluid flow induced by MHD on a vertical surface," *Symmetry*, vol. 15, no. 2, pp. 1–22, 2023.

[55] C. I. Christov, "On frame indifferent formulation of the Maxwell–Cattaneo model of finite-speed heat conduction," *Mechanics Research Communications*, vol. 36, pp. 481–486, 2009.